Chemistry Europe
European Chemical Societies Publishing

WILEY VCH

Excellence in Chemistry Research

Announcing our new flagship journal

- Gold Open Access
- Publishing charges waived
- Preprints welcome
- Edited by active scientists

Meet the Editors of *ChemistryEurope*

Luisa De Cola
Università degli Studi di Milano Statale, Italy

Ive Hermans
University of Wisconsin-Madison, USA

Ken Tanaka
Tokyo Institute of Technology, Japan

ChemCatChem

Research Article
doi.org/10.1002/cctc.202200356

Chemistry Europe
European Chemical Societies Publishing

www.chemcatchem.org

Nanometric-Thick Metal-Free h-Boron Nitride/Graphene Films as Base Catalyst for the Synthesis of Benzoxazoles

Alejandra Rendón-Patiño,[a] Ana Primo,[a] Bogdan Cojocaru,[b] Sabina Gabriela Ion,[b] Dana G. Popescu,[c] Vasile Parvulescu,*[b] and Hermenegildo García*[a]

Catalysts are frequently used as pelletized powdered materials, but rarely as thin films. The present work reports the use of 2D h-boron nitride on few layers defective graphene (h-BN/fl-G) films of about 10 nm thickness as base catalyst for the synthesis of benzoxazoles by coupling a 2-amino-phenol with *p*-substituted benzaldehydes. The synthesis of benzoxazole derivatives has aroused much interest in the last decades due to their application as potent anticancer agents against MCF-7 and MDA-MB-231 breast cancer cells. The results demonstrate that these nanometer-thick films exhibit three orders of magnitude higher activity than K_2CO_3 taken as benchmark base catalyst. The activity and selectivity of h-BN/fl-G films depend on the nature of substituents on benzaldehyde, the solvent and reaction temperature.

Introduction

Hexagonal boron nitride (h-BN) is a one-atom thick, 2D layer material structurally related to graphene with alternating B and N atoms in hexagonal arrangement.[1] Ideal h-BN nanosheets are commonly considered as an inert material.[2] In contrast of this lack of catalytic activity, it has been recently reported that h-BN is an active and selective catalyst for the oxidative dehydrogenation of propane to propylene with minimal CO_x selectivity.[3] Activation of h-BN can be achieved through defect generation by a post-synthetic treatment. For example, boron vacancies on as-synthesized h-BN results in surface exposed amino and hydroxyl groups that can act as basic centers on defective h-BN.[4] It would be of interest expanding the use of this nanometric material to other organic reactions requiring basic centers.

The interest on the use of 2D nanomaterials derives, in part, from the use as catalyst of nanometric-thick, continuous films, rather than much larger pelletized powders, or catalysts embedded in a polymeric membrane. In the case of nanometric graphene and related 2D materials, it should be possible to coat with a catalytically active thin film reactors or other materials.

In the present study we report the synthesis of benzoxazole using thin films of boron nitride supported on few-layers defective graphene (h-BN/fl-G) as catalyst in comparison with multi-layer h-BN powder. Benzoxazole derivatives have attracted considerable attention in the last decades due to the presence of this heterocycle in a variety of natural products, bioactive molecules and therapeutical compounds.[5] In this context, the usefulness of benzoxazoles as potent anticancer agents against MCF-7 and MDA-MB-231 breast cancer cell lines has been reported and confirmed.[6,7] One of the most general synthetic approach to prepare benzoxazoles involves condensation of 2-aminophenols with carboxylic acids or alcohols,[8] amines[9] ketones[10] and aldehydes[11] in the presence of an oxidant. Most of these reactions are carried out under strongly acidic conditions.[12,13]

The synthesis of benzoxazoles using aerobic oxidative conditions is catalyzed by various types of catalysts, including metal (Au, Pd, Cu nanoparticles), acid ($Cu(OTf)_2$, $TiCl_3OTf$), or oxidative organocatalyst, such as TEMPO. However, some of these catalysts work only for intramolecular reactions of either imines or carboxylic amides at high temperatures and even then, high catalyst loadings are required.[9,14,15–18]

Base catalysts have been much less investigated for benzoxazole syntheses. Among the few precedents, a study used commercial 5 Å molecular sieve [0.7 CaO:0.3 Na_2O:1.0 Al_2O_3:2.0 SiO_2:x H_2O] as presumed a base catalyst.[19]

Herein it will be reported that nanometer-thick films of single layer h-BN on few layers defective graphene films (*h-BN/fl-G films*) promote the synthesis of benzoxazoles by coupling a

[a] *Dr. A. Rendón-Patiño, Dr. A. Primo, Dr. H. García*
Instituto Universitario de Tecnología Química
Consejo Superior de Investigaciones Científicas-Universitat Politècnica de Valencia
Universitat Politècnica de Valencia
Av. De los Naranjos s/n
46022 Valencia (Spain)
E-mail: hgarcia@qim.upv.es
Homepage: https://hermenegildogarciagroup.es

[b] *B. Cojocaru, S. Gabriela Ion, Prof. V. Parvulescu*
Department of Organic Chemistry, Biochemistry and Catalysis
University of Bucharest
Blv. Regina Elisabeta nr.4-12, Sector 3
030016 Bucharest (Romania)
E-mail: vasile.parvulescu@chimie.unibuc.ro
Homepage: https://www.chimie.unibuc.ro/cercetare/cataliza/viparvulescu/index.html

[c] *D. G. Popescu*
National Institute of Materials Physics
Laboratory of Nanoscale Condensed Matter
405 A Atomistilor Str
077125, Magurele, Ilfov (Romania)

Supporting information for this article is available on the WWW under https://doi.org/10.1002/cctc.202200356

2-aminophenol with *p*-substituted benzaldehydes. Available CO_2 chemisorption measurements support that the catalytic activity of h-BN/fl-G films most likely derives from the presence of basic sites associated with the presence of atom vacancies in h-BN structure.

Results and Discussion

Preparation and characterization of h-BN/fl-G films

Preparation of the h-BN/fl-G films was performed following a procedure recently reported.[20] The process starts from commercial h-BN crystals that are exfoliated in CH_2Cl_2 by ultrasounds using polystyrene (MW_{av} 100 000 mau) as dispersing agent. The resulting dispersion is subsequently centrifuged at 1500 rpm and the supernatant was collected. This suspension is cast by spin coating onto a freshly cleaned quartz plate. After solvent evaporation at ambient temperature, the h-BN/polystyrene film is pyrolyzed under Ar flow at 900 °C. Scheme 1 illustrates the preparation procedure.

Figure 1 presents high resolution TEM images of the single layer h-BN on few layers defective graphene after detachment from the quartz plate. These images show that the films are constituted by crystalline h-BN sheets laying on top of graphene layers. Selected area electron diffraction patterns presented in Figure 1b confirm the superlattice structure of h-BN/fl-G films based on the coincidence of the diffraction points corresponding to the hexagonal pattern of h-BN with those of graphene. The superlattice configuration corresponds to the exact overlapping of the hexagonal lattice of h-BN coinciding on top of the hexagons of defective graphene. It has been proposed that this special superlattice configuration appears in the synthesis of the film due to the templating action of preformed h-BN sheets controlling the epitaxial growth of nascent defective graphene derived from polystyrene precursor.[20] Figure S1 in supporting information shows the XRD patterns of the h-BN/fl-G films used as catalysts in the present study. The single layer boron nitride on few-layers defective graphene deposited on quartz plates exhibits a low crystalline state with a broad diffraction line at 2θ of about 21.5° corresponding to the imperfect, loose packing of the graphene layers. The narrow diffraction lines at 44.1, 64.6 and 77.6 °, respectively, also observed in the XRD of the h-BN/fl-G films are due to the quartz support.

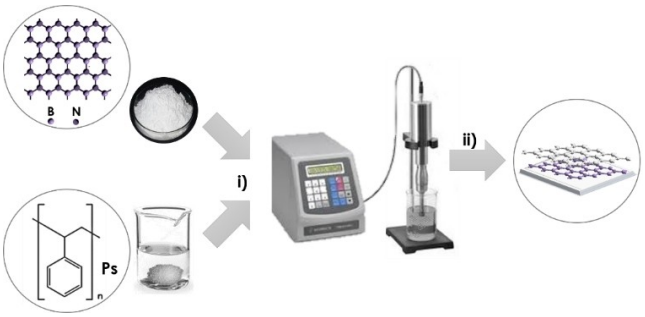

Scheme 1. Steps in the preparation of h-BN/fl-G films from commercial bulk h-BN crystals.

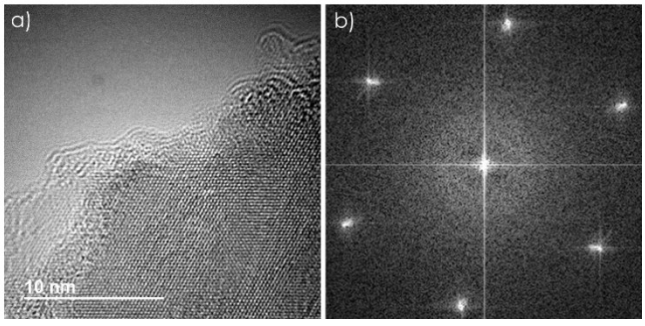

Figure 1. a) High resolution TEM images of h-BN/fl-G films detached from the quartz plate and b) the diffraction pattern confirming the superlattice structure of the h-BN/fl-G film by the coincidence of the diffraction points corresponding to h-BN and graphene hexagonal patterns. Note in the diffraction that each position of the hexagon has in reality two close points.

Figure 2 shows the high-resolution XP spectra of the h-BN/fl-G films in the regions of the C1s, O1s, N1s and B1s levels. For the C1s level (Figure 2a) the binding energies at 284.6 eV to graphene sp^2 carbons,[21,22] at 286.0 eV to carbon in C-OH,[23] C–O, C=C–O[24] and C–N[25] and at 288.1 eV to carbon in –COOH, –COOR and –COO– groups[24,25] For the O1s level (Figure 2b) the binding energy at 530.1 eV was assigned to the O–B bond[26] and at 532.7 eV to C–OH.[27] The N1s level (Figure 2c) has only one component with a binding energy at 398.9 eV corresponding to the expected value for boron nitride.[28] Similarly, the B1s level has a single component (Figure 2d) at a binding energy of 190.8 eV corresponding also to boron nitride.[29]

Quantitative analysis of the XPS peaks taking into account the response factor of each element indicated an atomic N/B

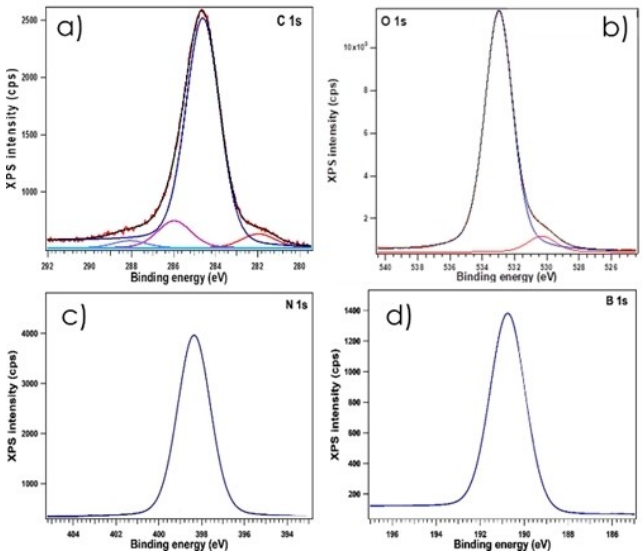

Figure 2. XP spectra of h-BN/fl-graphene films and the corresponding deconvolution of the different components a) C1 s; b) O1s; c) N1s; and d) B1s.

ratio of 1 in agreement with the expected stoichiometry of BN. The (N,B)/C atomic ratio of 0.11 indicates the large amount about 7–9 times of graphene in the film respect to BN. This is in agreement of the single layer h-BN arising from the exfoliation of bulk h-BN on top of few-layers graphene. This (N,B)/C atomic ratio is in agreement with the thickness of the h-BN/fl-G films determined by AFM (*vide infra*). The low O/C atomic ratio of 2.1×10^{-2} indicates that the oxygen content in the defective graphene is low in accordance with polystyrene composition as precursor of graphene. Worth noting is that the upper position of h-BN in the film can be deduced from the dependence of the quantitative elemental analysis by XPS with the monitoring angle. If instead of perpendicular to the film (90°), the analysis is carried out to lower angle values, then, an increase in the intensity of the B and N atoms, respect to C is observed. This dependence of the B/N vs. C atomic proportion with the detection angle has also previously taken as evidence of the upper location of h-BN layer respect to defective underneath graphene layers. Accordingly, the more electrons parallel to the h-BN/fl-G films are measured, the more correspond these electrons to the upper h-BN overlayer.

Raman spectroscopy allows differentiation between hexagonal and cubic boron nitrides.[30,31] The Raman spectra of commercial BN used as reference catalyst are presented in Figure 3. Hexagonal boron nitride (h-BN) is structurally related to graphite. In accordance, similarly to graphite, the weak lines at 1326 and 1636 cm^{-1} recorded in UV-Raman spectroscopy (excitation wavelength 325 nm) can be associated, respectively, to transverse TO and longitudinal LO phonon modes of graphitic h-BN. The presence in the same Raman spectrum of TO phonon scattering around 1119 cm^{-1} also accounts for the presence in the material of a cubic (c-BN) phase in commercial boron nitride.[32] Finally lines at 820 and 460 cm^{-1} are assigned to overtones of the measured phonon energies in h-BN. Thus, UV-Raman spectroscopy indicates that commercially available bulk multilayer BN is a combination of the hexagonal and cubic phases.

Raman spectra collected under visible excitation (wavelengths 488 or 633 nm, see also Figure 3) provide complementary information to that from UV. While preserving the typical lines of h-BN and c-BN, the spectrum collected at 488 nm makes more evident the presence of the graphitic, hexagonal structure of BN by recording the peaks located around 1580–1590 cm^{-1} and at 1350 cm^{-1}.[33] Also interesting, the splitting of the band at 1350 cm^{-1} recorded in the case of h-BN/fl-G may account for the presence of a single layer h-BN in the case of the h-BN/fl-G film.

The thickness of the h-BN/fl-G films was determined by AFM measurements and it was of about 10 nanometers. Representative measurements are presented in Figure 4. It seems that after pyrolysis of exfoliated h-BN embedded on polystyrene composite, a remarkable decrease in the thickness from micrometers for the polystyrene composite to nanometers for h-BN/fl-G films occurs. Frontal views show that the surface of the h-BN/fl-G films was smooth without the presence of cracks and crevices and significant roughness. These images agree with the superlattice overlap of h-BN on fl-G as deduced from electron diffraction images.

Catalytic tests

The results of the catalytic tests are summarized in Table 1. Synthesis of benzoxazoles by condensation of o-aminophenol and aldehydes has three main steps consisting of the imine formation that does not require any catalyst, irrespective of the solvent in which the reaction is carried out (Table 1, lines 1–4), intramolecular nucleophilic 5-endo cyclization of the OH group

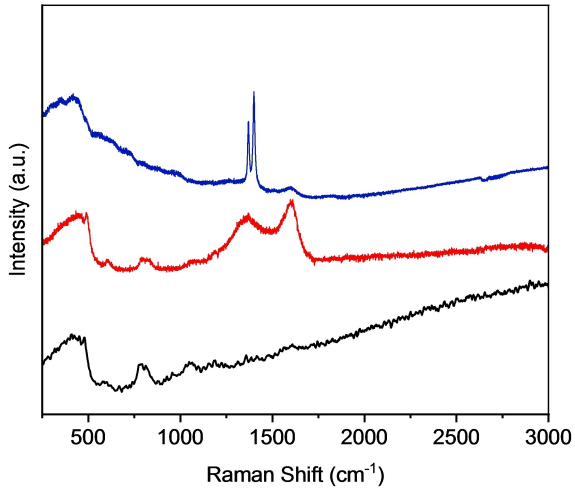

Figure 3. Raman spectra of commercial BN using laser excitation of 325 nm (black), 488 nm (red) and 633 nm (blue) showing that the solid contains the hexagonal and cubic phases.

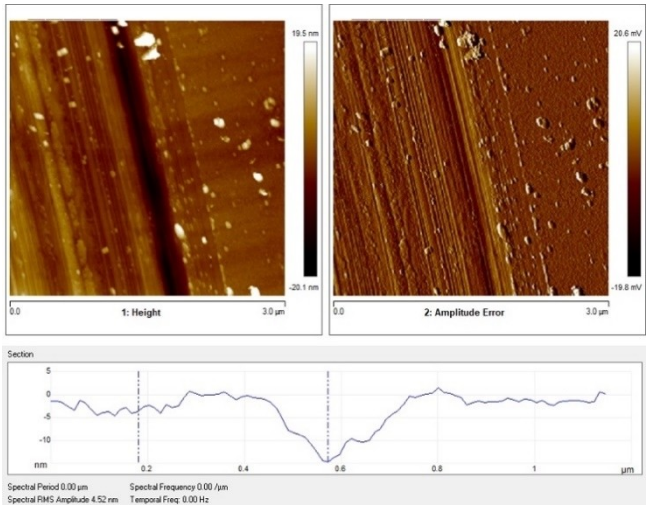

Figure 4. Upper images: Two frontal views by AFM of h-BN/fl-G films. The central line appearing in the views correspond to the cutter scratch used to determine film thickness. The small particles present in the images correspond to dust or debris from the material. Notice that the samples were not prepared in a clean room. The bottom plot shows the height profile along the cut observed in the frontal views. The film thickness was estimated as 11 nm.

Table 1. Conversion of benzaldehyde over the investigated catalysts.

Run	-R	Catalyst	Temp. [°C]	Solvent	Time [h]	Yield Benzoxazole [%]	TOF [s^{-1}]
1	$-NO_2$	No Catalyst	70	H_2O	2	0	0
2	$-NO_2$	No Catalyst	120	p-xylene	12	0	0
3	–Br	No Catalyst	70	H_2O	2	0	0
4	–Br	No Catalyst	120	p-xylene	12	0	0
5	–Br	K_2CO_3 (27.6 mg)	120	p-xylene	12	5.4	$6.2x10^{-6}$
6	–Br	K_2CO_3 (41.64 mg)	120	p-xylene	12	9.0	$6.9x10^{-6}$
7	–Br	K_2CO_3 (55.2 mg)	120	p-xylene	12	12.5	$7.2x10^{-6}$
8	–Br	K_2CO_3 (69.0 mg)	rt	p-xylene	12	1.9	$8.7x10^{-7}$
9	–Br	K_2CO_3 (69.2 mg)	120	p-xylene	12	15.8	$7.3x10^{-6}$
10	–Br	K_2CO_3 sonicated (69.2 mg)	120	p-xylene	12	33.6	$1.4x10^{-5}$
11	$-NO_2$	K_2CO_3 sonicated (69.2 mg)	120	p-xylene	12	2.4	$3.8x10^{-5}$
[12]	$-NO_2$	h-BN/fl-G films	rt	H_2O	2	7.0	$8.7x10^{-1}$
13	$-NO_2$	h-BN/fl-G films	70	H_2O	2	32.6	$4.1x10^{-2}$
14	$-NO_2$	h-BN/fl-G films	120	p-xylene	12	3.9	$4.9x10^{-3}$
15	–Br	h-BN/fl-G films	rt	H_2O	2	2.8	$3.5x10^{-3}$
16	–Br	h-BN/fl-G films	70	H_2O	2	9.0	$1.1x10^{-2}$
17	–Br	h-BN/fl-G films	70	p-xylene	2	35.4	$4.4x10^{-2}$
18	–Br	BN (10 mg)	120	p-xylene	12	32.4	$7.3x10^{-4}$
19	$-NO_2$	BN (10 mg)	120	p-xylene	12	55.9	$2.1x10^{-5}$
20	–Br 10μL HCl added	h-BN/fl-G films	70	H_2O	2	6.8	$0.8x10^{-5}$
21	–Br After 5 consecutive runs	h-BN/fl-G films	70	p-xylene	12	32.2	$3.0x10^{-5}$
22	–Br Inert Atmosphere	h-BN/fl-G films	120	p-xylene	12	22.1	$8.7x10^{-6}$

and the imine and final aromatization. Scheme 2 summarizes the elementary steps occurring in the formation of benzoxazole from o-aminophenol and benzaldehyde. Intramolecular cyclization is the slowest step in the process. The addition of a base like K_2CO_3 catalyzes the intramolecular cycloaddition of the phenolic oxygen to the imine intermediate by formation of the corresponding phenolate. The yields in the produced benzoxazole obey a linear dependence with the amount of the base catalyst in the reaction (Table 1, entries 5–11). It can be argued that the effect of K_2CO_3 as heterogeneous catalyst (Table 1) is limited due to the relatively small surface area (1.1 m^2g^{-1} after drying) in spite that the density of basic sites is similar to that of h-BN/fl-G (see below). Although we could not increase the surface area of K_2CO_3 upon grinding, ultrasound treatment for 3 h of K2CO3 increased its area to 1.7 m^2g^{-1}. The catalytic activity of ultrasound-treated K_2CO_3 in terms of TOF and benzoxazole yield increased respect to pristine sample (Table 1

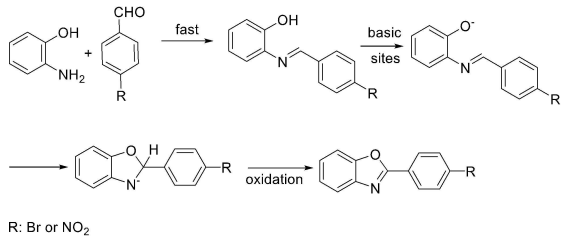

Scheme 2. The three elementary steps of the formation of 2-arylbenzoxazoles by condensation of o-aminophenol and benzaldehyde.

entries 10 and 11), indicating that surface area rather than the mass is the key factor.

Previous reports indicated that h-BN may have basic sites of strength $+9.3 > H > +7.2$, comparable to those of KY zeolite that has been used as base catalyst for the benzoxazole synthesis under current consideration.[34] In this regard, basicity and acidity has also been reported for h-BN due to the presence of atom vacancies [34] Thus, ball-milled h-BN powders showed high activity and selectivity toward β-nitroalkenes formation by Henry reaction and the Knoevenagel condensation.[34] This activity has been attributed to the presence of defects formed during ball milling of h-BN powders that generates acid and basic sites.

In line with these reports, it was found here that h-B*N/fl-G* films were able to promote benzoxazole formation (Table 1, entries 12–17, 20–22). Note that h-B*N/fl-G* films, although not unique, is one of the few examples of nanometric thin films exhibiting catalytic activity.

For the sake of comparison, the catalytic activity of h-BN/fl-G was compared with that of commercial, bulk, multilayer BN solid (Table 1, entries 18 and 19). Based on the chemisorption measurements, the TOF values presented in Table 1 show that sites on h-BN/fl-G film are at least one order of magnitude more active than those of bulk BN powder. The difference in the catalytic behavior between h-BN/fl-G and bulk multilayer BN powder is assumed to be due to the exposure of all atoms on the 2D film. This higher activity can be understandable considering the better availability of the basic sites on the h-BN/fl-G film.

It is proposed that the catalytic activity of *h-BN/fl-G* films is ascribed to basic sites associated to boron vacancies. This proposal is supported by NH_3 and CO_2 chemisorption measurements on the present *h-BN/fl-G* films. NH_3 as basic probe will serve to titrate acid sites on *h-BN/fl-G* films, while the number of basic sites can be determined in CO_2 chemisorption experiments. These measurements give values of 291.7 mmol/g for chemisorbed NH_3 and 694.5 mmol/g for chemisorbed CO_2 (Figure S2 in supporting information), indicating that the *h-BN/fl-G* films have acid/base sites. However, the density of basic sites is about 2.4 times higher than those of acid sites, indicating that h-BN/fl-G films contain predominantly basic sites. These basic sites can be ascribed to the presence of amino groups. These values contrast with ball-milled BN that contain both acid and basic sites,[34] while h-BN/fl-G is mainly a basic catalyst. In comparison, commercial BN contains 0.24 and 0.64 mmol g^{-1} of acid and basic sites, respectively, while the K_2CO_3 sample contains 0.1 mmol g^{-1} of basic sites.

In addition, the amount of h-BN in the films can be estimated knowing the amount of h-BN in the suspension after exfoliation and centrifugation. It was determined that the amount of h-BN was 3.8 $\mu g \times cm^{-2}$. Therefore the population of basic sites for the amounts of K_2CO_3 used as catalyst (27.6–69.2 mg) is much higher than those present in the h-BN/fl-G films ($2 \times 3.8\ \mu g \times cm^{-2}$). These quantitative measurements on the density of basic sites on *h-BN/fl-G* films can be used to determine the TOF values that can serve to rank the catalytic activity of these films respect to other conventional bases such as K_2CO_3. The TOF data are provided in Table 1.

To further support the role of basic sites, the condensation of 2-aminophenol and p-bromobenzaldehyde was performed in the presence of the h-BN*/fl-G* films upon addition of 10 μL HCl 35 %. A significant decrease in TOF and final benzoxazole yield was observed (Table 1, entry 20), providing an additional evidence on the nature of basic sites as catalytic centers.

In this way, turnover frequency (TOF) values as quantitative indicator of the catalytic activity shows that h-B*N/fl-G* films are far more active material than K_2CO_3 or bulk BN powders, considered as benchmark catalysts. The TOF values of benzoxazole formation from benzaldehyde derivatives achieved by *h-BN/fl-G* films are about three orders of magnitude higher than those measured for K_2CO_3 (see Table 1).

As expected in view of the relative electron withdrawing effect of nitro and bromo groups present on benzaldehyde reactivity, one of the factors affecting the yield of benzoxazole is the benzaldehyde substituent. As observed in Table 1, the TOF values for p-nitrobenzaldehyde are higher than those for the bromo derivative (Table 1, entries 18, 19 and 20). Other factor affecting the activity of *h-BN/fl-G* films is the solvent. It was observed that the reaction in water occurs with higher rates than in p-xylene (Table 1, entries 18–20, 23 and 24). This is in agreement with the intermediacy of anionic phenolate as the key reaction intermediate. In addition, the reaction temperature also affects the activity that increases as the temperature increases (Table 1, entries 18 and 19).

Finally, since the third step in the mechanism of benzoxazole formation is oxidation of the hydro precursor to form the aromatic oxazole heterocycle (see Scheme 1), an attempt to confirm the role of ambient oxygen as terminal oxidizing reagent was made by performing a control experiment under inert atmosphere in a glove box (Table 1, entry 22). Although formation of benzoxazole was still observed, probably due to the presence of oxygen in p-xylene and reagents, a significant decrease in the TOF value and benzoxazole yield was observed, thus, supporting ambient O_2 as the terminal oxidizing reagent in line with the current knowledge on benzoxazole formation previously reported.

Stability of h-BN/fl-G films as heterogeneous catalyst was confirmed by performing five consecutive reuses of the condensation of 2-aminophenol and 4-bromobenzaldehyde. After each run, the film was easily separated from the reaction mixture, washed with p-xylene and used in a consecutive run. Although a gradual slight decrease in activity was observed, the h-BN/fl-G was still active in the fifth run, decreasing 4-BrC_6H_4CHO conversion from 100 to 84 % and benzoxazole yield from 35.4 to 32.2 % (Table 1, entry 21). In addition, no changes in the XRD pattern of the fresh and five-times used h-BN/fl-G film was observed (Figure S3), indicating the structural stability of the thin film. Also elemental analyses by XPS and the components and binding energy values of the O1s, N1s and C1s peaks of five-times used h-BN/fl-G film remain unchanged in comparison to the analysis of the fresh films (Figure S4).

Conclusions

The present study has shown that nanometric thin h-BN/fl-G films can act as active and selective basic catalysts promoting the synthesis of benzoxazoles by coupling a 2-aminophenol with *p*-substituted benzaldehydes to form the corresponding benzoxazole. In agreement with the literature, basic sites generated by boron defects are the most likely active sites in the reaction. Comparison of the activity of h-BN/fl-G films with K_2CO_3 or BN powder as benchmark catalysts shows that nanometer-thick h-BN film is about three orders of magnitude more active for the reaction under study. Other factors controlling the benzoxazole yield are the nature of the benzaldehyde substituent, the solvent and the reaction temperature. It can be concluded that the best results are with the nitro-derivative, in water and at higher temperatures (120 °C). The h-BN/fl-G film as catalyst was reusable for five consecutive runs. Overall the present results show the potential of very thin (nanometric-thick films) as heterogeneous catalysts. These thin films can be deposited on inert substrates or can coat reactor wall thus allowing flexible reactor designs.

Experimental Section

Exfoliation BN and Preparation of h-BN/fl-G superlattice films

Commercial boron nitride (Aldrich,1.5 mg/mL) was added to a dichloromethane solution with polystyrene (Aldrich, 30 mg/mL). The mixture was sonicated using a tip sonicator with a sequence consisting of 1 s on and 1 s off for 3 h (FisherbrandTM Model 705,

700 W). The dispersion was then centrifuged at 1500 rpm for 45 min (Hettich Zentrifugen EBA 21) and the supernatant was preconcentrated to a total volume of 10 mL.

The films were finally deposited on 1×1 cm^2 quartz substrates using spin-coating technique (APT-POLOS spin-coater: 4000 rpm, 30 s). The pyrolysis of polystyrene treatment was performed using an electric oven and using the following heating program: heating at 5 °C/min at 900 °C for 2 h.

Physicochemical characterization

XRD patterns were obtained using a PANalytical Cubix-Pro diffractometer, which is equipped with a PANalytical X'Celerator detector. High resolution TEM (HRTEM) imaging was carried out with a JEOL JEM 2100F microscope operating at an accelerating voltage of 200 kV. Raman spectroscopy measurements were carried out using a Renishaw in Via Raman Microscope instrument at room temperature with a 514 nm Ar ion laser as excitation source coupled to a Lyca optical microscope.

Raman spectra were acquired in the extended spectral region from 150 to 4000 cm^{-1}. Raman analysis was carried out with a Horiba JobinYvon-Labram HR UV-Visible-NIR Raman Microscope using the excitation wavelengths at 325, 488, and 633 nm.

XPS were obtained on a SPECS spectrometer equipped with a Phoibos 150–9MCD detector using a non-monochromatic Al Kα X-ray source (1483.6 eV) operating at 50 W. Samples were evacuated into a spectrometer pre-chamber at 10^{-9} mbar. The quantification and processing of the spectra is carried out with CASA software, and the charge correction is done based on the carbon C 1s signal whose binding energy corresponds to the binding energy value of 284.5 eV.

Reaction procedure

All the catalytic tests were performed in 5 ml vials made of borosilicate glass. In a general procedure for the synthesis of the benzoxazole derivatives, 1 mmol of 2-aminophenol was reacted with 1 mmol of the corresponding benzaldehyde derivative in 2 ml of solvent, at temperatures between 25 and 80 °C, using 2×2 cm^2 h-BN/fl-G film as catalysts. Reference reactions were carried out with different loadings of K_2CO_3 as catalyst (27.6–69.2 mg) or bulk commercial multilayer BN powder. After the reaction time elapsed, the reaction mixture was cooled and a small aliquot was diluted for GC-MS analysis, the rest of the reaction mixture was filtered from the catalyst and slowly concentrated at 50 °C for ^{1}H- and ^{13}C-NMR spectra or FTIR analysis. When water was the reaction solvent, the reaction products were extracted three times with 10 mL aliquots of ethyl acetate. Conversion and selectivity of the products were calculated from GC-MS and the structure of the products confirmed by ^{1}H- and ^{13}C-NMR and FTIR spectroscopy. GC-MS analysis was carried out on a THERMO Electron Corporation instrument equipped with a TG-5SilMS column (30 m $\times$ 0.25 mm $\times$ 0.25 μm). The injector was set up at the temperature of 250 °C. The temperature in the oven was kept at 50 °C for 1 min and then increased up to 270 °C at a rate of 10 °C min^{-1}. ^{1}H-NMR spectra were collected on a Bruker Advance III UltraShield 500 MHz spectrometer, operating at 500.13 MHz for ^{1}H NMR, 125.77 MHz for ^{13}C NMR using TMS as internal standard in $CDCl_3$. FTIR spectra were recorded on Bruker Tenso-II FTIR spectrophotometer adapted with a Smart Accessory for diffuse reflectance measurements. Collected spectra represent the average of 32 scans, recorded at 4 cm^{-1} resolution. Powder of analyzed compound or mixture was diluted with KBr before each measurement.

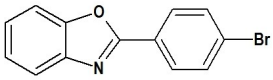

2-(4-Bromophenyl)benzoxazole: ^{1}H NMR (500 MHz, $CDCl_3$, ppm) δ 8.17–8.10 (m, 2H), 7.86–7.80 (m, 1H), 7.78–7.63 (m, 2H), 7.61–7.55 (m, 1H), 7.44–7.35 (m, 2H). ^{13}C NMR (125 MHz, $CDCl_3$, ppm) δ 162.1, 150.7, 142.0, 132.2, 129.0, 126.2, 126.1, 125.4, 124.8, 120.1, 110.6; GC-MS (EI, m/z) [M^+] 273, 275

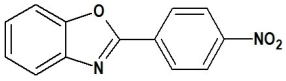

2-(4-Nitrophenyl)benzoxazole: ^{1}H NMR (500 MHz, $CDCl_3$, ppm) δ 8.46-8.43 (m, 2H), 8.41-8.38 (m, 2H), 7.85-7.79 (m, 1H), 7.71-7.65 (m, 1H), 7.47-7.40 (m, 2H) ^{13}C NMR (151 MHz, $CDCl_3$) δ 157.6, 151.3, 141.90, 132, 129.6, 128.7, 127.3, 125.2, 124.0, 119.9, 110.9. GC-MS (EI, m/z) [M^+] 240

The activity of the catalysts was expressed through turnover frequency values (TOF) calculated considering the population of the basic centers determined from the TPD measurements.

Acknowledgements

Financial support by the Spanish Ministry of Science and Innovation (Severo Ochoa and RTI2018-89237-CO2-R1), Generalitat Valenciana (Promoteo 2021–032) and UEFISCD (PN-III-P4-ID-PCCF-2016-0088, PN-III-P4-ID-PCE-2020-1532) is gratefully acknowledged. A. P. thanks the Ministerio de Ciencia e Innovación for a Ramón y Cajal research associate contract.

Conflict of Interest

The authors declare no conflict of interest.

Data Availability Statement

The data that support the findings of this study are available from the corresponding author upon reasonable request.

Keywords: Heterogeneous catalysis · Nanometer thin catalyst films · boron nitride film as catalyst · benzoxazol synthesis

[1] D. Golberg, Y. Bando, Y. Huang, T. Terao, M. Mitome, C. Tang, C. Zhi, *ACS Nano* **2010**, *4*, 2979–93.
[2] J. Dong, Q. Fu, H. Li, J. Xiao, B. Yang, B. Zhang, Y. Bai, T. Song, R. Zhang, L. Gao, *J. Am. Chem. Soc.* **2020**, *142*, 17167–74.
[3] W. P. McDermott, M. C. Cendejas, I. Hermans, *Top. Catal.* **2020**, 1–8.
[4] A. Takagaki, S. Nakamura, M. Watanabe, Y. Kim, J. T. Song, K. Jimura, K. Yamada, M. Yoshida, S. Hayashi, T. Ishihara, *Appl. Catal. A* **2020**, *608*, 117843.
[5] V. J. Ram, A. Sethi, M. Nath, R. Pratap, *The Chemistry of Heterocycles: Nomenclature and Chemistry of Three to Five Membered Heterocycles*, Elsevier, **2019**.

[6] M. B. Labib, J. N. Philoppes, P. F. Lamie, E. R. Ahmed, *Bioorg. Chem.* **2018**, *76*, 67–80.
[7] R. Chikhale, S. Thorat, R. K. Choudhary, N. Gadewal, P. Khedekar, *Bioorg. Chem.* **2018**, *77*, 84–100.
[8] X. Shi, J. Guo, J. Liu, M. Ye, Q. Xu, *Chemistry–A European Journal* **2015**, *21*, 9988–93.
[9] Y. Endo, J. E. Bäckvall, *Chemistry–A European Journal* **2012**, *18*, 13609–13.
[10] T. B. Nguyen, P. Retailleau, *Org. Lett.* **2017**, *19*, 3887–90.
[11] A. Patra, A. James, T. K. Das, A. T. Biju, *J. Org. Chem.* **2018**, *83*, 14820–6.
[12] F. Stephens, J. Bower, *Journal of the Chemical Society (Resumed)* **1949**, 2971–2.
[13] D. Hein, R. J. Alheim, J. Leavitt, *J. Am. Chem. Soc.* **1957**, *79*, 427–9.
[14] Y. Kawashita, N. Nakamichi, H. Kawabata, M. Hayashi, *Org. Lett.* **2003**, *5*, 3713–5.
[15] S. Ueda, H. Nagasawa, *Angew. Chem.* **2008**, *47*, 6511–3.
[16] S. Ueda, H. Nagasawa, *Angew. Chem.* **2008**, *120*, 6511–3; *Angew. Chem. Int. Ed.* **2008**, *47*, 6411–6413.
[17] Y. X. Chen, L. F. Qian, W. Zhang, B. Han, *Angew. Chem. Int. Ed.* **2008**, *47*, 9330–3; *Angew. Chem.* **2008**, *120*, 9470–9473.
[18] J. Azizian, P. Torabi, J. Noei, *Tetrahedron Lett.* **2016**, *57*, 185–8.
[19] W. Chang, Y. Sun, Y. Huang, *Heteroat. Chem.* **2017**, *28*, e21360.
[20] A. Rendón-Patiño, A. Doménech, H. García, A. Primo, *Nanoscale* **2019**, *11*, 2981–90.
[21] J. Waldrop, R. Grant, *Appl. Phys. Lett.* **1990**, *56*, 557–9.
[22] Y. Tan, Q. Gao, C. Yang, K. Yang, W. Tian, L. Zhu, *Sci. Rep.* **2015**, *5*, 1–11.
[23] A. Saha, S. Basiruddin, S. C. Ray, S. Roy, N. R. Jana, *Nanoscale* **2010**, *2*, 2777–82.
[24] V. C. Moore, M. S. Strano, E. H. Haroz, R. H. Hauge, R. E. Smalley, J. Schmidt, Y. Talmon, *Nano Lett.* **2003**, *3*, 1379–82.
[25] S. Reiche, R. Blume, X. C. Zhao, D. Su, E. Kunkes, M. Behrens, R. Schlögl, *Carbon* **2014**, *77*, 175–83.
[26] T. Arakawa, A. Saito, J. Shiokawa, *Applications of surface science* **1983**, *16*, 365–72.
[27] J. Pang, W. Jian, L. Wang, C. Wu, Y. Liu, J. He, X. Tang, *Carbohydr. Polym.* **2012**, *88*, 369–72.
[28] Y. Wang, Y. Shao, D. W. Matson, J. Li, Y. Lin, *ACS Nano* **2010**, *4*, 1790–8.
[29] G. Puyoo, F. Teyssandier, R. Pailler, C. Labrugère, G. Chollon, *Carbon* **2017**, *122*, 19–46.
[30] N. G. Chopra, R. Luyken, K. Cherrey, V. H. Crespi, M. L. Cohen, S. G. Louie, A. Zettl, *Science* **1995**, *269*, 966–7.
[31] T. Werninghaus, J. Hahn, F. Richter, D. Zahn, *Appl. Phys. Lett.* **1997**, *70*, 958–60.
[32] J. Sanjurjo, E. López-Cruz, P. Vogl, M. Cardona, *Phys. Rev. B* **1983**, *28*, 4579.
[33] I. Childres, L. A. Jauregui, W. Park, H. Cao, Y. P. Chen, *New developments in photon and materials research* **2013**, *1*, 1–20.
[34] S. Torii, K. Jimura, S. Hayashi, R. Kikuchi, A. Takagaki, *J. Catal.* **2017**, *355*, 176–84.

Manuscript received: March 12, 2022
Revised manuscript received: April 20, 2022
Accepted manuscript online: April 25, 2022
Version of record online: May 23, 2022